Yield stress aging in attractive colloidal suspensions

Francesco Bonacci, Xavier Chateau, Eric M Furst, Julie Goyon, Anaël Lemaître

Yield stress aging in attractive colloidal suspensions

Francesco Bonacci,[1] Xavier Chateau,[2] Eric M. Furst,[3] Julie Goyon,[2] and Anaël Lemaître[2]

[1] *PMMH, CNRS, ESPCI Paris, Université PSL, Sorbonne Université, Université de Paris, F-75005, Paris, France*
[2] *Navier, Ecole des Ponts, Univ Gustave Eiffel, CNRS, Marne-la-Vallée, France*
[3] *Department of Chemical and Biomolecular Engineering, University of Delaware, 150 Academy Street, Newark, Delaware, 19716, USA*

(Dated: January 20, 2022)

We investigate the origin of yield stress aging in semi-dense, saline, and turbid suspensions in which structural evolution is rapidly arrested by the formation of thermally irreversible roll-resisting interparticle contacts. By performing optical tweezer (OT) three-point bending tests on particle rods, we show that these contacts yield by overcoming a rolling threshold, the critical bending moment of which grows logarithmically with time. We demonstrate that this time-dependent contact-scale rolling threshold controls the suspension yield stress and its aging kinetics. We identify a simple constitutive relation between the contact-scale flexural rigidity and rolling threshold, which transfers to macroscopic scales. This leads us to establishing a constitutive relation between macroscopic shear modulus and yield stress that is generic for an array of colloidal systems.

Our understanding of aging in colloidal suspensions has been guided for decades by studies of transparent sterically stabilized experimental models [1, 2] in which van der Waals forces are absent and contact formation excluded. In such systems, aging results from a slow (glass-like) microstructural evolution [3, 4]. But most colloidal suspensions in the environment, industry, or civil engineering, are saline and turbid. Turbidity signals the existence of an index contrast between particles and suspending fluid, i.e., of *attractive* van der Waals forces; salinity introduces ions that screen particle charges, thus weakening the repulsive Coulombic forces. These two properties hence conspire to facilitate the formation of solid-solid interparticle contacts.

It was very recently pointed out that moderate levels of ionic strength and index contrast suffice to bias the balance between Coulombic repulsion and van der Waals attraction to the point that no repulsive barrier limits the formation of adhesive, roll-resisting, and thermally stable interparticle contacts, with the consequence that, at intermediate (30% to 40%) packing fractions, the microstructure freezes within seconds of flow arrest [5]. These systems, however, do present mechanical aging on timescales up to hours [6–9], much beyond structural arrest. For a broad class of real-life suspensions, mechanical aging is hence non-structural, and governed by contact scale physical processes.

Identifying these processes is a major challenge, requiring joint advances in experiments (spotting and characterizing the relevant contact scale processes) and theory (modeling them and deducing macroscopic properties). Macroscopic shear modulus (G') aging can be related to the growth of contact-scale flexural rigidity [5]. But, the most crucial issue in most practical situations, the mechanism of macroscopic yield stress (σ_y) aging, is wide open.

Most yield stress models for suspensions [10, 11] indeed assume interactions to be centro-symmetric, hence cannot offer any insight as to how roll-resisting contacts determine macroscopic modulus and yield stress aging. Interparticle roll-resisting contacts were experimentally shown to yield by overcoming a rolling threshold [12], but no experimental evidence exists for microscopic yield aging in adhesive contacts between colloidal particles. And no direct, quantitative, link has ever been established between contact and macroscopic yielding in any attractive colloidal suspension.

Here, we address these interrelated issues by investigating yielding at both the macroscopic and contact scales in aqueous suspensions of Stöber silica particles flocculated by $CaCl_2$ at moderate ionic strengths (I). By performing three-point OT bending tests on particle rods, we show that contacts yield when reaching a rolling threshold, and that the associated critical bending moment M_y ages. We demonstrate that this contact-scale process controls macroscopic yield stress aging as $\sigma_y(t_w) \propto M_y(t_w)/a^3$ with t_w the age and a the particle radius. It leads us to identify a constitutive relation between the macroscopic shear modulus and yield stress $\sigma_y(t_w) \propto \sqrt{G'(t_w)}/a$, the prefactor being a material-dependent constant of unit $\mathrm{N}^{1/2}$. Our finding entails that it is possible to track the growth of the yield stress by monitoring the shear modulus, an observation with far-reaching consequences for real-life situations.

Interparticle contacts are probed using Pantina and Furst's method [13, 14], a three point OT bending test on a rod comprising an odd number of particles (see Fig. 1a). During a test, two fixed traps hold the rod extremities; a third one grabs the central particle before being translated perpendicularly to the rod, at a velocity slow enough to avoid hydrodynamic drag effects. Sample preparation and measurement protocol follow the Method section of Ref. [5] except otherwise stated.

Here, we perform these tests using particles of diameter $2a = 1.9\,\mu\mathrm{m}$. At all the considered ionic strengths, interparticle contacts are thermally stable [5] and cannot be opened by pulling the particles apart with optical traps. Consistently, the maximum force OT's can exert ($\simeq 15\mathrm{pN}$), which is ~ 3 times larger than those we will use here, is much smaller than the Derjaguin-

Muller-Toporov (DMT) [15] estimate for the pull-off force, $\pi a W \simeq 24\,\mathrm{nN}$, with W the work of adhesion [16].

Force and deflection measurements rest on image analysis with subpixel resolution [17]. Before each test, the average trap stiffness k is measured by monitoring the thermal fluctuations of particles held by the three traps. Once the rod formed, before loading, the average positions of both end particles are measured to identify the end trap locations. These two points defines the x axis. Loading is performed along the transverse horizontal axis, denoted y. The force exerted on the central particle is obtained, in essence, as $f = k(\Delta y_1 + \Delta y_N)$, with Δy_1 and Δy_N the y-displacements of both end particles from the end trap locations. Finally, the rod deflection δ is measured as the difference between the y coordinates of the center and end particles. In practice, rods are not strictly linear: the associated misalignments are corrected by analyzing the 3D rod structures [5].

Typical force vs deflection data are reported in Fig. 2a, for a few aging times (t_w), as counted starting from the formation of the last bond in the assembly process.

At small deflections, rods respond elastically with f increasing essentially linearly with δ. Meanwhile, the rod deformation is well-described by the Euler-Bernoulli beam equation (solid blue line in Fig. 1b), which entails that contacts support finite torques, i.e., resist rolling [5]. The associated effective bending rigidity is $k_0 = 8(N-1)^3 f/\delta$, with N the number of beads. Modelling the rod as a series of beads connected by roll-resisting contacts, yields the contact scale flexural stiffness $k_r = k_0 a^2/\Gamma$ with $\Gamma \simeq 96$ a slightly N-dependent parameter [18]. These stiffnesses grow quasi-logarithmically with time [5], which attests to the existence of contact-scale aging dynamics.

With the increasing deflection, yielding eventually occurs, quite abruptly, without any evidence of incipient plastic activity, at a yield point (f_y, δ_y). Immediately afterwards (Fig. 1a,b, green data), the rods systematically display a triangular shape, which evidences that a single contact (the apex, with abscissa $x^\star$), has rolled. Noticeably, the rods do not break open after yielding.

To shed light on the yielding mechanism, we perform a large number of tests and report the $x^\star$ distribution in Fig. 1c. If yielding resulted from frictional sliding, the distribution of $x^\star$ would be uniform, because the shear force along a bent rod is. In contrast, we find that yield events occur overwhelmingly at $x^\star = \pm a$, i.e., in the contacts formed by the central particle, which is where the local moment $M_y = (f_y/2)\,[L/2 - |x^\star|]$ is maximal. These data hence unambiguously demonstrate that yielding results from the crossing of a rolling threshold [12].

Accordingly, the rare yield events occurring away from the center particle must be attributed to experimental artifacts, such as contact-scale defects or poorly formed rods. Therefore, in order to carry out a quantitative, time-resolved analysis of roll yielding, we only retain the $x^\star = \pm a$ events, and report M_y vs t_w in Fig. 2b. Remarkably, M_y grows roughly logarithmically at late times, like the flexural stiffness k_r does [5]. It is also essentially I-independent over the studied I range, over which the charge carried by our particles is constant [5, 9].

It was never previously reported that the contact scale rolling threshold grows logarithmically in time. This ob-

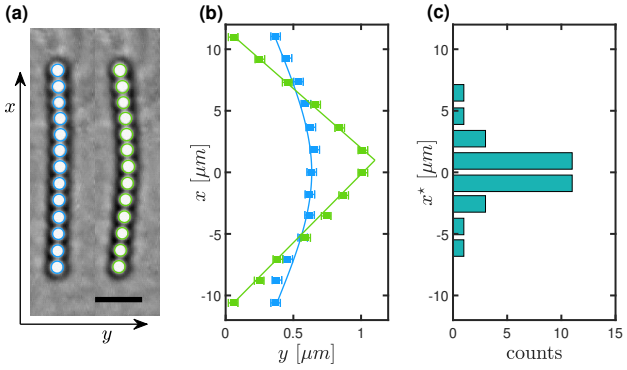

FIG. 1. (a) Two snapshots of a 13 silica particle rod, just before and just after a yielding event. The colored circles show the particle positions as reconstructed from subpixel image analysis (radii are reduced for better legibility). Scale bar = 5 µm. (b) The reconstructed particle positions in the (x, y) plane, superposed, after magnification along the y axis. Pre-yielding positions (blue) agree with the Euler-Bernoulli equation (line); post-yielding ones (green) form two straight segments connected at a finite angle. (c) Distribution of first yield event locations ($x^\star$): $\sim 70\%$ occur near the rod center, where the bending moment is maximum.

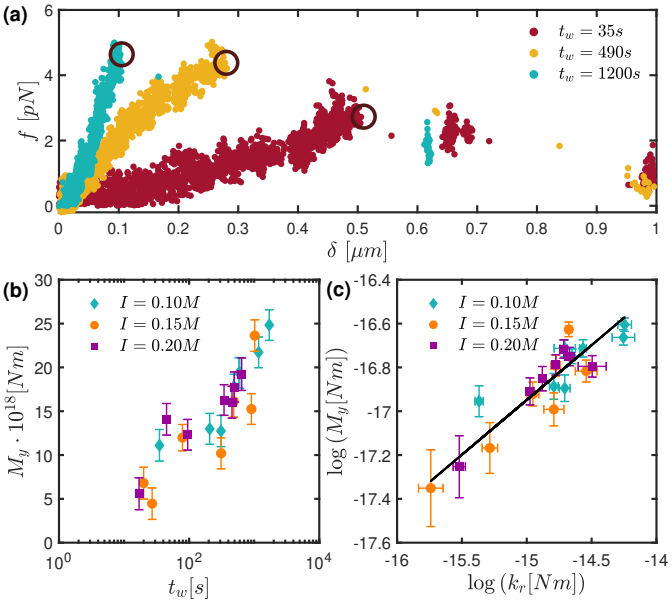

FIG. 2. (a) Typical bending force (f) vs deflection (δ) curves after three aging times. Circles mark the yield points (f_y, δ_y). (b) Log-lin plot of the critical bending moment (M_y) versus aging time (t_w). Error bars are deduced from measurement uncertainties in f_y and $x^\star$. (c) Critical moment (M_y) versus flexural stiffness (k_r) for all t_w and I.

servation hence constitutes a key experimental finding about adhesive colloidal suspensions.

Plotting M_y vs k_r as parametrized by t_w [Fig. 2c], we find that these two contact properties quite nicely obey the relation (solid line)

$$M_y = g\, k_r^{\alpha} \tag{1}$$

with $\alpha = 1/2$ and $g = (3.56 \pm 0.3) \cdot 10^{-10}\mathrm{N}^{1/2}\mathrm{m}^{1/2}$. This relation implies that the critical bending angle $\theta_y = M_y/k_r = g/\sqrt{k_r}$ decreases with t_w, i.e. that *contacts become increasingly brittle as they age*. This is directly visible in Fig. 2a as δ_y clearly decreases with t_w. It points to a contact yield mechanism (contact line depinning) akin to fragile rupture.

In this OT study, we focused on a single particle size, due to the difficulties in accumulating data points. While g is a priori a-dependent, the proximity of the measured exponent α to $1/2$ suggests it might be prescribed by simple physical principles, with the scaling $M_y(t_w) = g \times [k_r(t_w)]^{1/2}$ constituting a generic property of the contacts between microspheres. We explore this issue in the rest of the paper.

For a contact to resist rolling, its contour must remain pinned. Its flexural rigidity, which results from elastic strains inside the particles, is determined by the contact geometry. Flexural aging hence demonstrates that the contact radius a_c grows. Following Furst *et al* [13], we estimate $k_0 = 12\pi E a_c^4/a^3$ [19], the bending stiffness of a rod of diameter a_c and Young's modulus E, which yields:

$$k_r = \frac{12\pi E a_c^4}{a\Gamma} \tag{2}$$

This a_c^4 scaling is supported by shear modulus aging data for a range of particle sizes [5]. It arises because flexion introduces a linear stress $\sigma \propto \theta\, y$ throughout the contact area A_c (y being the bending direction), so that integrating the associated torque yields $\int_{A_c} \mathrm{d}y\mathrm{d}z\, y\sigma \sim a_c^4\,\theta$.

The growth of a_c points to a type of sintering process (e.g. the progressive formation of siloxane bridges [20–22]), which increases the overall cohesion energy inside the contact area. Thus, here, adhesion results from two distinct types of interactions: van der Waals attraction and intra-contact bonds formed by sintering. The former is time-independent and invariant under particle rotations: it brings about contact formation and adhesion, yet *does not introduce rolling resistance*, which is why contacts do not display measurable flexural rigidity immediately after they form [5]. Intra-contact bonding is time-dependent and begets rolling resistance.

We construct a schematic description of such a contact, in the spirit of contact theories [23], all of which relate the contact diameter to the adhesion energy W via:

$$a_c(t_w) = A\left(\frac{3\pi\, a^2\, W(t_w)}{8E^*}\right)^{1/3} \tag{3}$$

with $E^* = E/(1-\nu^2)/2$ the reduced modulus, $E = 30\,\mathrm{GPa}$ [24], $\nu = 0.17$ the Poisson's ratio [25]. For our aging contacts, W should be interpreted as a t_w-dependent effective adhesion energy, which integrates all adhesive forces inside the contact. The precise value of A, $= 1$—resp. $3^{1/3} \simeq 1.44$—in DMT—resp. Johnson–Kendall–Roberts (JKR) [26]—theories, is irrelevant to our analysis.

Next, rolling requires contact line depinning, a fragile rupture mechanism. Namely [27], it takes place when the strain energy release rate during rolling, ΔG, equals the adhesion hysteresis ΔW, i.e. the difference between the surface creation and opening energies at the leading and trailing edges (resp.). After calculating ΔG as a function of the bending level for a JKR contact, Krijt *et al* [27] thus obtain the following yielding criterion

$$\theta_y(t_w) = \frac{a_c(t_w)\,\Delta W}{6\,a\,W(t_w)} \tag{4}$$

where we explicitly show all t_w-dependencies. In Krijt *et al*'s calculation, W appears via the global condition of zero total force: it corresponds to the $W(t_w)$ of Eq. (3), which integrates all age-dependent adhesive contributions throughout the contact. In contrast, we expect the adhesion hysteresis ΔW to be t_w-independent because (i) the closing energy obviously is; (ii) the opening energy too since opening occurs at the rim of the growing contact where sintering has not taken place yet.

In our model, the contact state is set by $a_c(t_w)$, with the effective adhesion energy $W(t_w) \sim a_c^3(t_w)$ [Eq. (3)]. Equation (4) then yields $\theta_y(t_w) \sim 1/a_c^2(t_w)$, all coefficients being constant. Since $k_r(t_w) \sim a_c^4(t_w)$ [Eq. (2)], we obtain $\theta_y(t_w) \sim 1/\sqrt{k_r(t_w)}$, or $M_y(t_w) \sim \sqrt{k_r(t_w)}$, i.e. Eq. (1) with the prefactor:

$$g = \frac{(3\pi)^{3/2} A^3 (1-\nu^2)\Delta W}{12\sqrt{\Gamma E}}\sqrt{a} \tag{5}$$

Using $A^3 = 3$ (JKR), the measured $g \simeq 3.56 \cdot 10^{-10}\mathrm{N}^{1/2}\mathrm{m}^{1/2}$ corresponds to $\Delta W \simeq 77\,\mathrm{mJ/m^2}$, a fairly reasonable value [28], which provides compelling support to our argument.

For a fixed microstructure, we expect the shear modulus [5] and yield stress to be proportional to the flexural stiffness k_r and critical moment M_y respectively. For dimensional reasons, these relations read:

$$G'(a,\phi,t_w) = \frac{S(\phi)}{a^3} \times k_r(a,t_w) \tag{6}$$

$$\sigma_y(a,\phi,t_w) = \frac{Q(\phi)}{a^3} \times M_y(a,t_w) \tag{7}$$

where S and Q, which characterize the frozen microstructure, are independent of time, particle size, and ionic strength.

Equation (7) offers us an opportunity to test our theoretical analysis of the contact problem, which predicts the

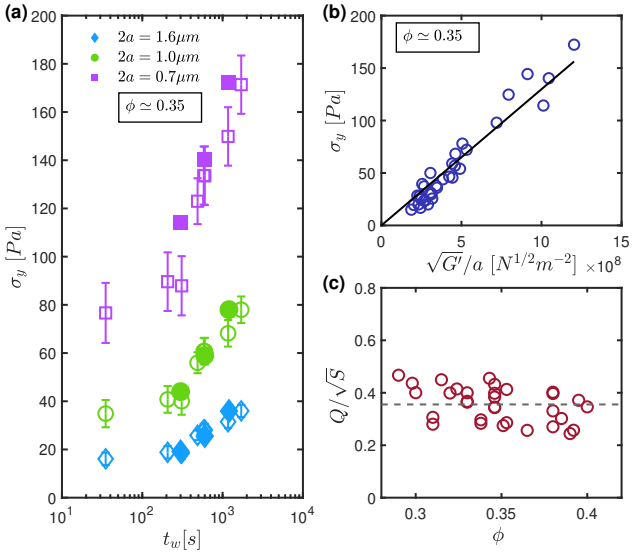

FIG. 3. (a) Macroscopic yield stress (filled symbols) of $\phi \simeq 0.35$ suspensions as measured from rheology stress sweep tests. Open symbols (in corresponding colors) are the predictions obtained from Eq. (8) using the single value $Q \simeq 0.9$ for all three series of points. (b) Test of the macroscopic constitutive relation [Eq. (9)]: σ_y vs $\sqrt{G'}/a$ for all $\phi \simeq 0.35$ suspensions, with $2a$ ranging from 0.7 to 1.6 µm and I from 0.1 to 0.2 M. The solid line is not a fit, but the prediction of Eq. (9) using the ϕ-average value of $Q/\sqrt{S} \sim 0.355$ from panel (c) and the fitted value of $g(a^\star)/\sqrt{a^\star}$. (c) $Q/\sqrt{S}$ as a function of ϕ, obtained from independent fits of Q and S by matching microscopic and macroscopic data.

non-trivial scaling $M_y(a, t_w) \sim W^{2/3}(t_w)\, a^{4/3}$. This cannot be done directly using OTs due to the limited range of accessible particle sizes. But, together with Eq. (7), it predicts that, for two different radii a and $a^\star$:

$$\sigma_y(a, \phi, t_w) = \frac{Q(\phi)}{a^3} \left(\frac{a}{a^\star}\right)^{4/3} M_y(a^\star, t_w) \qquad (8)$$

which expresses the macroscopic threshold of suspensions of arbitrary a as a function of $M_y(a^\star, t_w)$.

We have systematically tested this relation against rheometry data [9]. Like M_y, σ_y does not depend on I, but strongly grows with ϕ over the studied range. A typical test is presented in Fig. 3a. Filled symbols represent $\sigma_y(t_w)$ for $\phi \simeq 0.35$ suspensions, at $t_w = 300$, 600, 1200 s, and for $2a = 0.7$, 1.0, and 1.6 µm. As seen, σ_y increases with t_w and decreases with a. Equation (8) predicts that all these data points can be reconstructed from our $M_y(a^\star, t_w)$ OT data, with $2a^\star = 1.9\,\mu$m [Fig. 2], using a *single* fitting parameter Q. This highly constrained fit yields the three series of open symbols: it works remarkably well, thus bringing clear support to our analysis.

Combining Eqs. (1), (5), (6) and (7), we now obtain

$$\sigma_y(a, \phi, t_w) = C(\phi)\, \frac{\sqrt{G'(a, \phi, t_w)}}{a} \qquad (9)$$

which is a constitutive relation between the macroscopic shear modulus and yield stress of an aging suspension. Here, $C(\phi) = (g(a)/\sqrt{a})\, Q(\phi)/\sqrt{S(\phi)}$ is a function of ϕ only since $g/\sqrt{a}$ only depends on physical properties of the particles [Eq. (5)]. Equation (9) is tested in Fig. 3b where we plot σ_y vs $\sqrt{G'}/a$ for $\phi \simeq 0.35$ and an otherwise broad range of conditions ($2a$ from 0.7 to 1.6 µm, I from 0.1 to 0.2 M). The agreement is remarkable.

We have successfully tested Eqs. (8) and (9) for various packing fractions over the range (from $\phi \simeq 0.3$ to 0.4) over which our suspensions are stable and present a measurable yield stress [**?**]. We are thus able to estimate $Q(\phi)$ and $S(\phi)$ independently: the former, by matching Eq. (8) as in Fig. 3; the latter via a similar analysis of G' and k_r data [5]. The resulting values of $Q(\phi)/\sqrt{S(\phi)}$, displayed in Fig. 3c, do not show any systematic ϕ-dependence. This is quite meaningful, despite the limited accessible packing fraction range, because the parameters $S(\phi)$ and $Q(\phi)$ vary separately by significant factors: S from 1.9 to 47 (a factor of $\simeq 25$), and Q from 0.5 to 2.5 (a factor of 5).

To rationalize our observations, let us emphasize that, since contacts form within seconds of flow arrest, their relative age differences decrease with time. Moreover, despite experimental difficulties, our $k_r(t_w)$ data [5] show strikingly moderate sample-to-sample fluctuations. Hence, in a suspension at rest, beyond a short transient, all contacts essentially present the same $k_r(t_w)$. Meanwhile, normal stiffnesses are essentially infinite.

Therefore, when a suspension microstructure responds elastically, the microscopic non-affine motions are age-independent: at macroscopic strain γ, for any contact ij, the flexion angle $\theta_{ij} = A_{ij}\gamma$, with A_{ij} constant. In a system of volume V, the energy density is $\frac{1}{2V}\sum_{ij} k_r A_{ij}^2 \gamma^2$, the sum running over all contacts; the elastic modulus $G' = \frac{N_c}{V}\langle A_{ij}^2\rangle\, k_r$, with N_c the number of contacts and $\langle\cdot\rangle$ the ensemble average. Since the studied phenomenon takes place in a limited packing fraction range, away from jamming, we may write $N_c/V \simeq \rho/a^3$, with ρ a constant of order a few units, which yields Eq. (6) with $S = \rho\langle A_{ij}^2\rangle$.

We found above contacts to be brittle, and increasingly so with age. Yet, suspensions are ductile: their yielding hence requires that of a measurable fraction of contacts precipitating a drop in the elastic modulus. Under such yielding conditions, the rescaled moment $\sqrt{\langle\theta_{ij}^2\rangle}/\theta_y(t_w) = \kappa$ should achieve a constant value. Therefore, the yield strain $\gamma_y = \kappa\theta_y/\sqrt{\langle A_{ij}^2\rangle}$ and $\sigma_y = G'\gamma_y = (1/a^3)\sqrt{\rho S}\kappa M_y$. We now recover Eq. (7) while predicting $Q/\sqrt{S} = \kappa\sqrt{\rho}$ to be a constant, just as shown by our data.

In summary, we have brought compelling evidence that adhesive colloidal suspensions yield by a mechanism that depends on interparticle contacts reaching an age-dependent rolling threshold associated with the depin-

ning of the contact line, a brittle rupture mechanism. We have identified a microscopic constitutive relation [Eq. (1)] relating this threshold to the flexural stiffness and were able to explain its origin within a model which, although schematic, is fully consistent with both our previous interpretation of the origin of flexural rigidity [5] and an existing estimate of the rolling threshold [27]. This model, moreover, predicts a non-trivial particle size dependence of the macroscopic yield stress, which we successfully tested.

This led us to identify a macroscopic constitutive relation between the yield stress and shear modulus [Eq. (9), with C a constant], which constitutes a major outcome. It opens two perspectives of considerable practical interest: identifying non-destructive probes of the age-dependent yield stress of suspensions, the most important property in many situations; or controlling the yield stress (and shear modulus) by altering the surface chemistry of particles.

[1] T. C. B. McLeish, M. E. Cates, J. S. Higgins, P. D. Olmsted, M. L. Kilfoil, E. E. Pashkovski, J. A. Masters, and D. A. Weitz, Philosophical Transactions of the Royal Society of London. Series A: Mathematical, Physical and Engineering Sciences **361**, 753 (2003).

[2] C. J. Dibble, M. Kogan, and M. J. Solomon, Phys. Rev. E **74**, 041403 (2006).

[3] B. Abou, D. Bonn, and J. Meunier, Phys. Rev. E **64**, 021510 (2001).

[4] L. Cipelletti and L. Ramos, Journal of Physics: Condensed Matter **17**, R253 (2005).

[5] F. Bonacci, X. Chateau, E. M. Furst, J. Fusier, J. Goyon, and A. Lemaître, Nature Materials (2020).

[6] P. Coussot, H. Tabuteau, X. Chateau, L. Tocquer, and G. Ovarlez, Journal of Rheology **50**, 975 (2006).

[7] N. Roussel, G. Ovarlez, S. Garrault, and C. Brumaud, Cement and Concrete Research **42**, 148 (2012).

[8] G. Ovarlez and P. Coussot, Phys. Rev. E **76**, 011406 (2007).

[9] J. Fusier, J. Goyon, X. Chateau, and F. Toussaint, Journal of Rheology **62**, 753 (2018).

[10] P. J. Scales, S. B. Johnson, T. W. Healy, and P. C. Kapur, AIChE Journal **44**, 538 (1998).

[11] R. J. Flatt and P. Bowen, Journal of the American Ceramic Society **89**, 1244 (2006).

[12] J. P. Pantina and E. M. Furst, Langmuir **24**, 1141 (2008).

[13] J. P. Pantina and E. M. Furst, Phys. Rev. Lett. **94**, 138301 (2005).

[14] J. P. Pantina and E. M. Furst, Langmuir **22**, 5282 (2006).

[15] B. Derjaguin, V. Muller, and Y. Toporov, Journal of Colloid and Interface Science **53**, 314 (1975).

[16] $W \simeq \frac{A_H}{12\pi D_0^2} \approx 8\,\mathrm{mJ/m^2}$, with $A_H = 8.3 \times 10^{-21}\mathrm{J}$ the non-retarded Hamaker constant of silica in water, and estimating the surface-surface separation at contact to be $D_0 = 0.165\,\mathrm{nm}$ [30].

[17] J. C. Crocker and D. G. Grier, Journal of Colloid and Interface Science **179**, 298 (1996).

[18] V. Becker and H. Briesen, Phys. Rev. E **78**, 061404 (2008).

[19] L. Landau and E. Lifshitz, *Theory of Elasticity: Volume 7*, Course of theoretical physics (Elsevier Science, 1986).

[20] B. Gauthier-Manuel, E. Guyon, S. Roux, S. Gits, and F. Lefaucheux, Journal de physique **48**, 869 (1987).

[21] G. Vigil, Z. Xu, S. Steinberg, and J. Israelachvili, Journal of Colloid and Interface Science **165**, 367 (1994).

[22] Y. Liu and I. Szlufarska, Phys. Rev. Lett. **109**, 186102 (2012).

[23] E. Barthel, Journal of Physics D: Applied Physics **41**, 163001 (2008).

[24] J. Paul, S. Romeis, J. Tomas, and W. Peukert, Advanced Powder Technology **25**, 136 (2014).

[25] Even large changes in ν have little effect on a_c as $1/(1-\nu^2)^{1/3}$ varies from 1 to 1.1 when ν varies from 0 to 0.5. We can thus safely use an average value for fused silica's Poisson ratio [24].

[26] K. L. Johnson, K. Kendall, and A. D. Roberts, Proceedings of the Royal Society of London A: Mathematical, Physical and Engineering Sciences **324**, 301 (1971).

[27] S. Krijt, C. Dominik, and A. G. G. M. Tielens, Journal of Physics D: Applied Physics **47**, 175302 (2014).

[28] For a typical surface energy of silica in water $W_0 \simeq 100\,\mathrm{mJ/m^2}$ [29], this yields $\Delta W/W_0 \simeq 0.77$, while Krijt et al [27] report $\Delta W/W_0$ values ranging between 0.5 and 1 for silica.

[29] K. Iler, *The Chemistry of Silica: Solubility, Polymerization, Colloid and Surface Properties and Biochemistry of Silica* (John Wiley and Sons Inc, 1979) p. 896.

[30] J. N. Israelachvili, in *Intermolecular and Surface Forces (Third Edition)*, edited by J. N. Israelachvili (Academic Press, San Diego, 2011) third edition ed., pp. 415 – 467.